Environmental Science & Technology

Article

Cite This: Environ. Sci. Technol. 2019, 53, 10352−10360

pubs.acs.org/est

Cooperative Pollutant Adsorption and Persulfate-Driven Oxidation on Hierarchically Ordered Porous Carbon

Chiheng Chu,[†,⊥,#] Ji Yang,[‡,§,#] Dahong Huang,[†] Jianfeng Li,[§] Aiqin Wang,[*,‡] Pedro J. J. Alvarez,[∥,⊥] and Jae-Hong Kim[*,†,⊥]

[†]Department of Chemical and Environmental Engineering, Yale University, New Haven, Connecticut 06520-8286, United States

[‡]State Key Laboratory of Catalysis, Dalian Institute of Chemical Physics, Chinese Academy of Sciences, Dalian 116023, China

[§]State Key Laboratory for Physical Chemistry of Solid Surfaces and MOE Key Laboratory of Spectrochemical Analysis and Instrumentation, iChEM, College of Chemistry and Chemical Engineering, Xiamen University, Xiamen 361005, China

[∥]Department of Civil and Environmental Engineering, Rice University, Houston, Texas 77005, United States

[⊥]Nanotechnology-Enabled Water Treatment (NEWT), Yale University, 17 Hillhouse Ave, New Haven, Connecticut 06511, United States

Supporting Information

ABSTRACT: This study presents a 3D hierarchically ordered porous carbon material (HOPC) that simultaneously achieves efficient adsorption of a range of water pollutants as well as catalytic oxidation of adsorbed pollutants. High adsorption capacity and rapid adsorption kinetics are attributed to the hydrophobic nature of the carbon substrate, the large surface area due to high porosity, and the relatively uniform size of pores that comprise the structure. The oxidative degradation is achieved by efficient mediation of electron transfer from pollutants to persulfate through the sp^2-hybridized carbon and nitrogen network. As the persulfate activation and pollutant oxidation do not involve reactive radicals, oxidative degradation of the adsorbent is prevented, which has been a primary concern when adsorption and oxidation are combined either to regenerate adsorbate or to enhance oxidation performance. Batch tests showed that near complete removal of various recalcitrant micropollutants can be achieved within a short time (less than 1 min) even when treating a complex water matrix, as pollutants are concentrated on the surface of HOPC, where their oxidation is catalyzed.

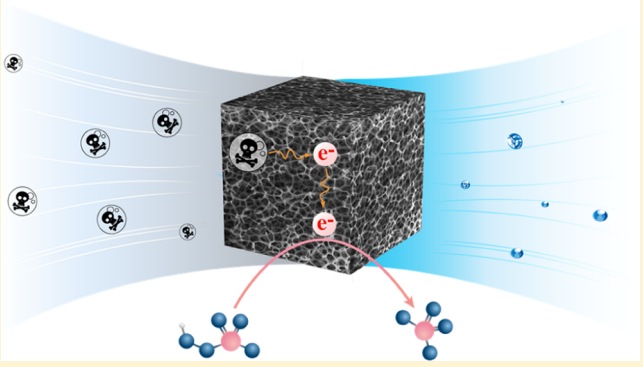

INTRODUCTION

Coupling adsorption and advanced oxidation, two widely used water treatment technologies, have been an appealing idea pursued by many researchers. While the adsorption effectively removes a wide range of anthropogenic pollutants from water,[1,2] the pollutants are merely transferred from one phase to another rather than being transformed to harmless end products. Destroying the adsorbed pollutants and regenerating adsorbents require additional treatments, such as thermal pyrolysis[3] or organic solvent washing,[4] which raise secondary environmental concerns. The adsorbed pollutants can be oxidatively degraded, even mineralized, by oxidative radicals [e.g., hydroxyl radicals ($^{\bullet}$OH) and sulfate radical ($SO_4^{\bullet-}$)] that are in situ-generated in an advanced oxidation process (AOP). Combining the AOP with adsorption can lead to a significant increase in treatment efficiency, especially when catalytic oxidation is executed on the surface of the adsorbent[5,6] where pollutants are concentrated (i.e., in a strategy known as hook and destroy[7−10]). One critical limitation in this scheme is the oxidation of adsorbents by nonselective reactive radicals leading to loss of the adsorption property because most high-adsorption-capacity adsorbents are carbon-based (e.g., activated carbon). Inorganic adsorbents such as zeolites are resistant to oxidation,[11] but they exhibit inferior adsorption performance compared to organic adsorbents.[12]

We find persulfate-based oxidation that relies on the nonradical oxidation pathway which is an interesting alternative. The persulfate-driven process generally targets *en masse* production of $SO_4^{\bullet-}$ by activation of a persulfate precursor such as peroxymonosulfate (PMS) and peroxydisulfate (PDS), collectively termed persulfate. Persulfate is cost-effective,[13] applicable at a wide pH range, and easy to transport and store,[13,14] making it a viable alternative to hydrogen peroxide, a precursor for $^{\bullet}$OH in conventional AOP. When the

Received: May 22, 2019
Revised: August 1, 2019
Accepted: August 6, 2019
Published: August 6, 2019

DOI: 10.1021/acs.est.9b03067
Environ. Sci. Technol. 2019, 53, 10352−10360

persulfate is applied along with structured carbocatalysts with abundant sp^2-hybridized carbon atoms [e.g., zero-dimensional nanodiamonds (ND),[15] one-dimensional carbon nanotubes (CNT),[16−18] two-dimensional reduced graphene oxide (rGO)[19]], pollutants (electron donor) that can be oxidized as persulfates (electron acceptor) are reduced to sulfate without involving sulfate radical generation.[15−21] These carbocatalysts not only provide a surface to harbor the electron donor/transfer pair but also efficiently mediate electron transfer through their conjugated system.[15,17]

Previously explored nanostructured carbocatalysts unfortunately have a relatively small surface area (e.g., ∼240 m^2/g for ND and CNT),[15] often much smaller than commercial activated carbon (e.g., ∼500−1000 m^2/g),[4] and have a tendency to aggregate in water.[22−24] To address this challenge, we here synthesize a 3D hierarchically-ordered porous carbon material (HOPC) that exhibits a large surface area and abundant adsorption sites. The network of uniform pores in this material prevents aggregation and ensures efficient mass transport—and therefore rapid adsorption—of target pollutants.[22−24] In addition, high contents of sp^2-hybridized C and N in the backbone structure promotes the electron transfer from the pollutant to persulfate, leading to rapid decomposition of adsorbed pollutants. Because no free radicals are generated during this process, the oxidation and destruction of the adsorbent is avoided. We demonstrate the superior performance of HOPC for adsorbing and degrading a range of recalcitrant pollutants of public concern, including bisphenol A (BPA; a plastic additive), sulfamethoxazole (SMX, a pharmaceutical), 17α-ethinylestradiol (EE; a pharmaceutical), 4-chlorophenol (CP; a pesticide), 2,4,6-trichlorophenol (TCP; a fungicide), and asulam (ASU; an herbicide) in water with interfering species such as natural organic matter (NOM).

MATERIALS AND METHODS

Catalyst Synthesis. HOPC was synthesized by polymerizing 2,6-diaminopyridine[25] on a SiO_2 template. Briefly, 2,6-diaminopyridine (5.5 g) was dissolved in water (400 mL) containing colloidal silica (30 g) under bath ultrasonication for 30 min, followed by the addition of NaOH (1.1 g) and ammonium persulfate (18.57 g dissolved in 100 mL water). The mixture was stirred for 12 h under an ice bath, separated by filtration, washed with water, and dried at 120 °C overnight. The powder obtained was ground, heated at 200 °C for 1 h and at 800 °C for 2 h in a tube furnace under N_2 gas. Finally, the SiO_2 template was removed by etching in 10% HF solution.

CNT and rGO were surface functionalized with amine groups to promote their persulfate-activation activity.[26] CNT or rGO (0.5 g) was dispersed in a concentrated nitric acid (60 mL) and sulfuric acid (20 mL) mixture for 3 h. Afterward, the mixture was slowly diluted with water under an ice bath. The oxidized CNT and rGO were separated by centrifugation, washed with ethanol (twice) and water (twice), freeze-dried at −60 °C, and redispersed in ethanol under ultrasonication for 30 min, followed by the addition of 2 mL (3-aminopropyl)-triethoxysilane to oxidized CNT suspension or aminopropyl-trimethoxysilane to oxidized rGO suspension. After stirring for 12 h, amine-modified CNT and rGO were centrifuged, washed with ethanol (twice) and water (twice), freeze-dried, and collected for further experiments.

Catalyst Characterization. Scanning electron microscopy (SEM) images were taken with a Hitachi S5500 scanning electron microscope operated at 30 kV. Transmission electron microscopy (TEM) images were taken using a JEM-2100F field emission electron microscope (JEOL, Japan). HOPC samples were prepared by ultrasonication in ethanol and dripping on a TEM Cu grid. Size and zeta potential characterizations were conducted using a Zetasizer Nano ZS with a 4 mW He−Ne laser operated at 633 nm. Nitrogen sorption isotherms were obtained by degassing carbocatalyst samples at 120 °C for 1 h and at 250 °C for 12 h followed by performing the adsorption using Micromeritics ASAP2010 at −196 °C. The Brunauer−Emmett−Teller (BET) surface area was deduced from an analysis of the isotherm in the relative pressure range of 0.05−0.3 for N_2. The total pore volume was calculated from the amount of nitrogen adsorbed at a relative pressure of 0.95. X-ray diffraction (XRD) analysis was carried out on a PANalytical X'pert diffractometer using nickel-filtered Cu Kα radiation with a scanning angle (2θ) of 5°−90°, operated at 40 kV and 40 mA. XPS measurements were operated at 15 kV and 10.8 mA using a ESCALAB 250 X-ray photoelectron spectrometer microprobe (Thermo Scientific, USA) coupled with an Al anode (Al Kα = 1846.6 eV). A survey analysis was performed across the entire energy range and higher resolution analyses in the N 1s, C 1s, and O 1s regions. Energy calibration was carried out using the C 1s peak of adventitious C at 284.6 eV.

Adsorption Measurement. Batch experiments were performed to assess the sorption of micropollutants to carbocatalysts. Catalysts (0.6 mg) were dispersed in water (3 mL) under ultrasonication for 30 min, followed by the addition of 50 μM of each micropollutant (i.e., BPA, SMX, EE, CP, TCP, ASU; the log K_{ow} and pK_a values of micropollutants are summarized in Table S1). The suspensions were vortexed, and small aliquots (150 μL) were removed at designated time points, immediately centrifuged, and the aqueous supernatants were taken for further analysis. Concentrations of micropollutants were analyzed using Agilent high-performance liquid chromatography coupled to a photodiode array detector. The composition of the mobile phase, UV absorption wavelength, and retention time for analysis of each pollutant species are summarized in Table S2.

Degradation Measurement. Degradation of the micropollutant was assessed using the same suspension used in adsorption measurement. The reaction was initiated by adding 1−20 μL PMS (100 mM; PMS is chosen over PDS because PMS has been more frequently used with carbonaceous materials in past studies). Small aliquots (130 μL) were removed at designated time points, mixed with 20 μL KI (100 mM to quench the unreacted PMS), centrifuged, and the supernatants were collected. Pollutants that potentially remain adsorbed to catalysts were recovered by ultrasonicating the suspension in acetonitrile for 10 s, centrifuging, and collecting the acetonitrile supernatant. BPA degradation was further assessed under complex water conditions in the presence of NOM (Suwannee River NOM, Lot 2R101N, purchased from the International Humic Substances Society), synthetic drinking water, synthetic seawater, or wastewater treatment plant effluent catchment. The recyclability of HOPC was assessed by repetitive addition of BPA and PMS up to six cycles. The long-term effectiveness of HOPC was evaluated by assessing BPA degradation in HOPC suspensions that were aged by adding 2 mM PMS daily for two weeks.

DOI: 10.1021/acs.est.9b03067
Environ. Sci. Technol. 2019, 53, 10352−10360

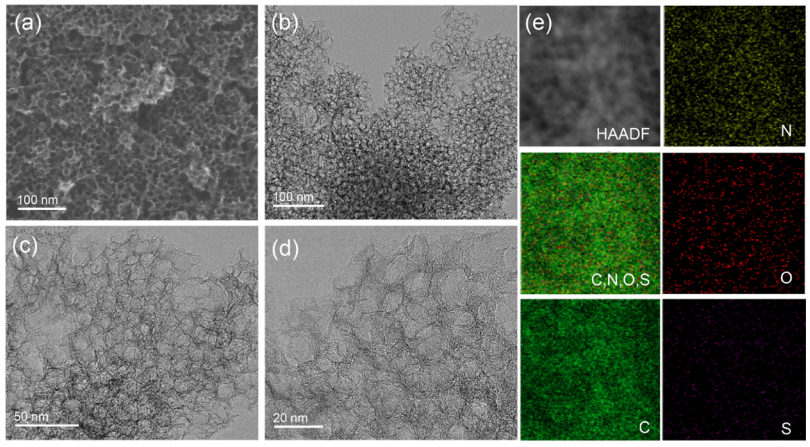

Figure 1. Microscopic characterization of HOPC using (a) SEM, (b–d) high-resolution TEM, and (e) EDS element mapping.

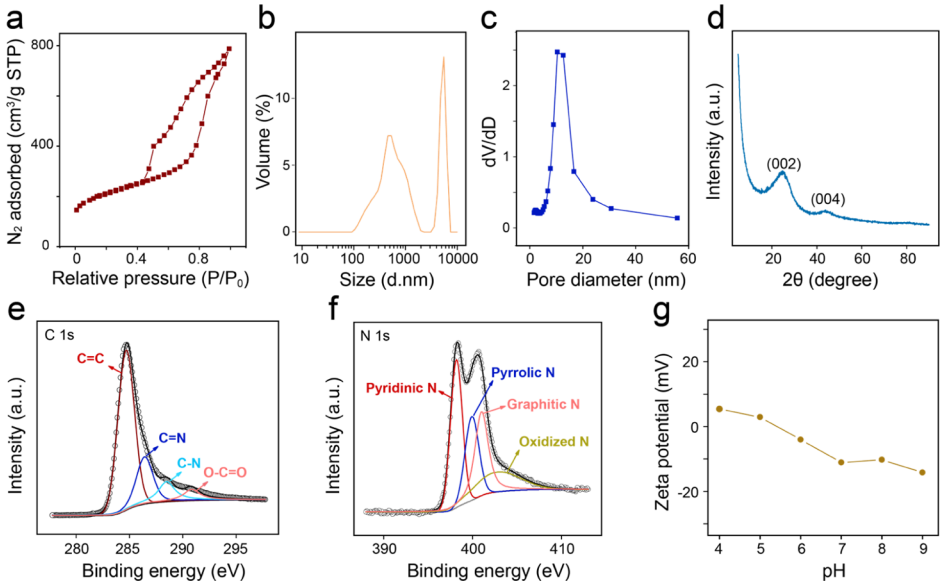

Figure 2. (a) N_2 adsorption–desorption isotherms of HOPC. (b) Size distribution of HOPC in pure water. (c) Size distribution of mesopores in HOPC. (d) XRD pattern of HOPC. (e–f) Binding energy of C 1s and N 1s for HOPC by high-resolution XPS. (g) Zeta potentials of HOPC at different solution pHs.

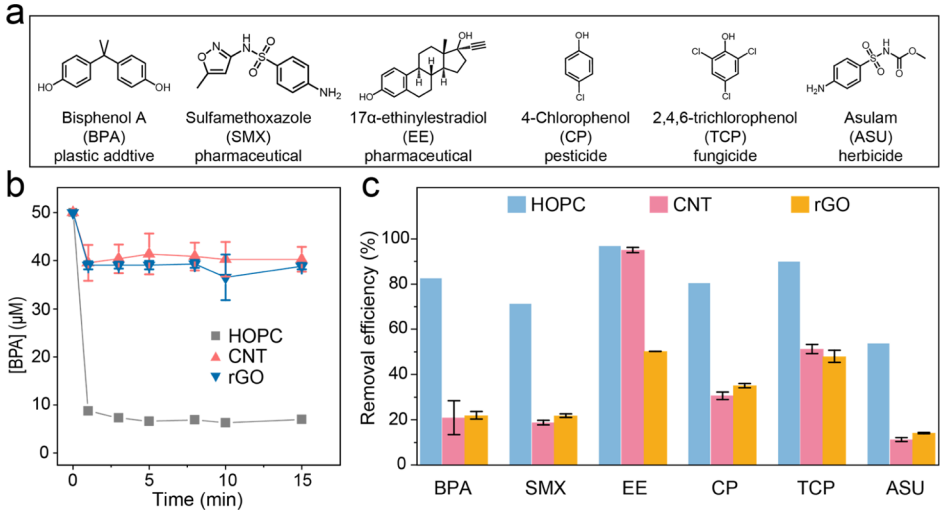

Figure 3. (a) Structures of select micropollutants. (b) Adsorption kinetics of BPA by carbocatalysts. (c) Efficiency of adsorptive removal of micropollutants by carbocatalysts after 1 min. In all experiments, [micropollutant] = 50 μM, [carbocatalyst] = 0.2 g/L, T = 20 °C, and pH = 7.4.

DOI: 10.1021/acs.est.9b03067
Environ. Sci. Technol. 2019, 53, 10352–10360

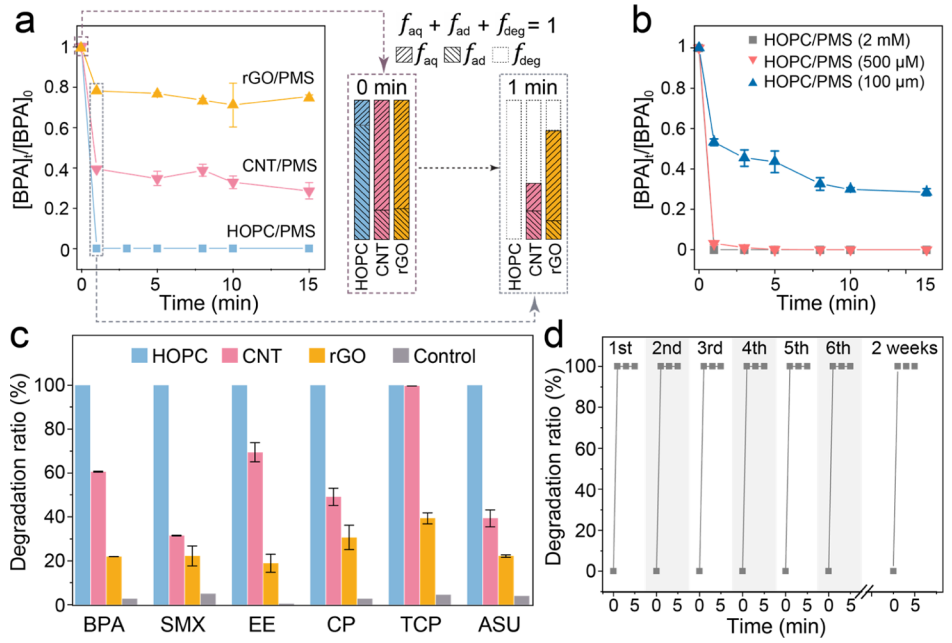

Figure 4. (a) Degradation kinetics of BPA in carbocatalyst suspensions. The inset illustrates the fractions of different BPA forms at 0 and 1 min after PMS addition. The remaining BPA ($[BPA]_t/[BPA]_0$) was divided into two fractions: carbocatalyst-adsorbed fraction (f_{ad}) and freely-dissolved fraction (f_{aq}). (b) BPA degradation in HOPC suspensions with varying concentrations of PMS (from 100 μM to 2 mM). (c) Degradation of micropollutants in carbocatalyst suspensions after 1 min reactions. Pollutant degradation in the control experiment without the carbocatalyst was assessed after 5 min reactions. (d) Repetitive use of HOPC for catalyzing degradation of BPA. In each cycle, 50 μM BPA and 2 mM PMS were added. In all experiments, [micropollutants] = 50 μM, [carbocatalysts] = 0.2 g/L, PMS = 2 mM, T = 20 °C, and pH = 3.5.

RESULTS AND DISCUSSION

HOPC Exhibited High Surface Area and Porosity. SEM images show the hierarchically ordered and porous structure of as-prepared HOPC (Figure 1a). The high porosity of HOPC was confirmed by TEM images (Figure 1b–d) and large pore volume (1.1 cm^3/g) obtained by BET measurement. As-prepared HOPC exhibited a large surface area (702 m^2/g; Figure 2a), which is comparable to commercial activated carbon (e.g., 507 m^2/g for activated carbon used in point-of-use filters[4]) and much larger than CNT (170 m^2/g) and rGO (98 m^2/g). The average size of HOPC in pure water was determined to be 375 nm by the size analyzer (Figure 2b). Nitrogen gas adsorption isotherm indicates that HOPC has a narrow pore size distribution that peaked at 11 nm (Figure 2c), which agreed well with the TEM characterization (~10 nm; Figure 1b–d). Energy-dispersive X-ray spectrometry (EDS) images suggest that N was uniformly distributed across the HOPC surface (Figure 1e).

C and N Atoms in HOPC Were sp^2-Hybridized. XRD peaks were located at 25° and 43°, corresponding to the (002) and (004) planes of graphitized C matrix (Figure 2d).[27] This agreed well with XPS measurements, where C in the as-prepared HOPC mainly existed in sp^2-hybridized form (Figure 2e). The successful integration of sp^2-hybridized N in the HOPC backbone structure was confirmed by the distinct C═N bond (Figure 2e) and N 1s peaks (Figure 2f) that were mainly comprised as follows: graphitic (i.e., sp^2-hybridized N neighbored with three sp^2-C; peaks at 401.0 eV), pyridinic (i.e., N in a six-atom heterocyclic ring; peaks at 398.1 eV), and pyrrolic N (i.e., N in a five-atom heterocyclic ring; peaks at 400.0 eV).[28,29] The O–C═O peak indicates the existence of carboxylic groups, albeit minor, which is likely induced by oxidation during NaOH/persulfate treatment or annealing during the catalyst synthesis. The zeta potential analysis shows that the surface charge of HOPC decreased from +5.4 to −14.2 mV as pH increased from 4.0 to 9.0 (Figure 2g), which is likely due to deprotonation of pyridinic N, pyrrolic N, and carboxylic groups.

Micropollutant Adsorption. HOPC exhibited a high capacity for rapid adsorption of multiple pollutants with varying functionalities (Figures 3a and S1). For instance, >95% of BPA adsorption equilibrium was reached within 1 min (Figure 3b), which is much faster than commercial activated carbon (typically >5 min to reach equilibrium[4]). At equilibrium, HOPC adsorbed >85% of BPA (i.e., 50 $mg_{BPA}/g_{catalyst}$). In comparison, CNT and rGO only adsorbed 21 and 22%, respectively, of BPA at equilibrium (Figure 3b). HOPC also outperformed CNT and rGO for adsorption of other select pollutants by a significant margin (Figure 3c). The high adsorption capability of HOPC is attributed not only to high surface area resulting from its porous structure but also to its relatively uniform pore size that makes most of its surfaces available for sorption of target molecules. Adsorption of investigated pollutants to HOPC is likely caused by strong $\pi-\pi$ stacking and hydrophobic effect, two well-documented sorption driving forces in the interaction of aromatic compounds with sp^2-hybridized carbon materials.[22] SMX and ASU showed the lowest adsorption by HOPC among tested pollutant species. Given that HOPC is also negatively charged at circumneutral pH (Figure 2g; zeta potential = −11.8 mV at pH 7.0), the lower adsorptions of SMX and ASU were likely caused by electrostatic repulsion because SMX (pK_a = 5.6) and ASU (pK_a = 4.8) are also negatively charged. Notably, the decreased solution pH with PMS addition may deplete the charge of HOPC (Figure 2g), SMX, and ASU, leading to suppressed electrostatic repulsion and enhanced adsorption of SMX and ASU. TCP (pK_a = 6.2) is also negatively charged but showed relatively higher adsorption because TCP has much

DOI: 10.1021/acs.est.9b03067
Environ. Sci. Technol. 2019, 53, 10352–10360

less negative charge and higher hydrophobicity (log K_{ow} = 3.7) compared to SMX (log K_{ow} = 0.9) and ASU (log K_{ow} = −0.3).

Micropollutant Degradation. When PMS was added, HOPC exhibited superior performance for catalyzing oxidative degradation of multiple micropollutants. Here, initially added micropollutants can be separated into three fractions (Figure 4a, inset): carbocatalyst-adsorbed fraction (f_{ad}, physically adsorbed fraction, measured after the recovery with acetonitrile), freely dissolved fraction (f_{aq}), and degraded fraction (f_{deg}). The fraction of degraded micropollutants was assessed by subtracting the fractions of remaining micropollutants, both the adsorbed form and dissolved form from initially added pollutants (i.e., $f_{deg} = 1 - f_{ad} - f_{aq}$). In other words, $[BPA]_t$ in Figures 4a,b, 6a, and 7 represents the sum of two fractions: the carbocatalyst-adsorbed fraction and the dissolved fraction.

The suspension pH decreased from 7.4 to 3.5 with addition of 2 mM PMS. Control experiments with only PMS and without the carbocatalyst show a slight degradation of micropollutants (Figure S2; up to 5% of micropollutant degradation in 5 min). The slow yet noticeable degradation of micropollutants agrees with recent findings that phenolic and anilinic compounds can be slowly oxidized by direct reaction with PMS, where PMS acts as an electrophilic oxidant.[30] When CNT or rGO were added to the solutions, micropollutant degradation was significantly accelerated (Figure 4a). Note that a sizable fraction of the pollutant remained physically adsorbed on CNT and rGO. In comparison, when HOPC was added, all select pollutants reached 100% degradation within 1 min, and no fraction remain physically adsorbed (i.e., all pollutants that adsorbed to HOPC was destroyed). This degradation was accompanied by significant decrease in the amount of total organic carbon (e.g., 76% of carbon in BPA was mineralized in 60 min; Figure S4), suggesting CO_2 as the main oxidation product (i.e., mineralization). Even with very low concentration of PMS (i.e., 100 μM) compared to the typically practiced dose (i.e., 1−10 mM), >50% degradation of BPA was achieved in 5 min (Figure 4b). Notably, while HOPC only adsorbed ASU by 55% at equilibrium (Figure 3c), it catalyzed the fast and complete degradation of ASU (Figure 4c) when PMS was added, suggesting the cooperative effect of simultaneous adsorption and oxidative degradation.

HOPC Durability. The durability of HOPC was demonstrated by its high and stable performance for catalyzing BPA degradation through repetitive use up to six cycles (Figure 4d). Further, the effectiveness of HOPC for catalyzing BPA degradation was preserved after aging in PMS for two weeks (Figure 4d). We attribute the high durability of HOPC to the nature of the HOPC/PMS system that does not involve radical generation (see additional discussions below). XPS measurements confirmed that HOPC was not oxidized. No decrease in C and N contents or increase in the O content was observed for HOPC after repetitive use when compared to the control (i.e., HOPC incubated in Na_2SO_4 solution) (Figure 5). In comparison, when incubated in the presence of Co^{2+}, a catalyst well known for activating PMS to $SO_4^{\bullet-}$,[31,32] HOPC was oxidized as indicated by a much enhanced C═O peak, decreased N content, and increased O content (Figure 5). While HOPC itself did not catalyze any radical production, transition metal ions in the reduced state could facilitate radical generation following the similar mechanism induced by Co^{2+} and potentially induce oxidation of HOPC over long-term application.

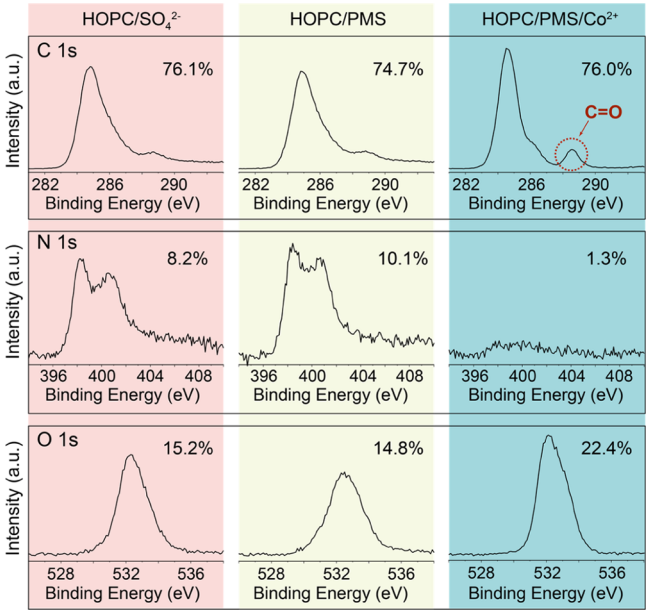

Figure 5. Binding energy of C 1s, N 1s, and O 1s for HOPC measured by high-resolution XPS. For the HOPC/SO_4^{2-} sample, HOPC was incubated in 2 mM Na_2SO_4 for 1 week. In the HOPC/PMS system, HOPC was repeatedly used by addition of 100 μM BPA and 2 mM PMS for six cycles, and stored for another week. For the HOPC/PMS/Co^{2+} sample, HOPC was incubated in the presence of 100 μM BPA, 2 mM PMS, and 2 mM Co^{2+} for one week. The composition of each element is presented as the atomic percentage. All HOPC samples were washed with methanol (three times) and water (three times), and dried in a vacuum oven (50 °C) overnight before XPS measurements.

Pollutants Degrade through HOPC-Mediated Electron Transfer to PMS. The fact that HOPC is not affected during the oxidation of organic pollutants results from a unique two-electron transfer mechanism that does not involve radical species. We first observed that adding methanol (2%, v/v), a radical scavenger (second-order rate constant = 2.5×10^7 and 9.7×10^8 M^{-1} s^{-1} for $SO_4^{\bullet-}$ and $^{\bullet}OH$, respectively[33,34]), did not affect BPA degradation in the HOPC/PMS system (Figure 6a). In comparison, BPA degradation performance of the Co^{2+}/PMS system, a well-known system to generate $SO_4^{\bullet-}$ as a major reactive species through the one-electron transfer process,[31,32] was significantly suppressed by adding methanol (Figure 6a). The absence of radical generations in the HOPC/PMS system was further supported by the nondetectable degradation of benzoic acid (Figure 6b), a widely used radical probe (Text S2; second-order rate constant = 1.2×10^9 and 4.2×10^9 M^{-1} s^{-1} for $SO_4^{\bullet-}$ and $^{\bullet}OH$,[35] respectively).[17,18,36−38] This was in stark contrast to full degradation of benzoic acid in the Co^{2+}/PMS system. Finally, when terephthalic acid (TPA) was added as a radical probe (Text S3), we did not observe the formation of hydroxyterephthalic acid (hTPA) as the product of radical-mediated hydroxylation of TPA.[39] In the Co^{2+}/PMS system, TPA was readily converted to hTPA (Figure 6b). The above results collectively suggest negligible radical generations in the HOPC/PMS system.[15]

We attribute the rapid degradation of micropollutants in the HOPC/PMS system to direct electron transfer from micropollutants (electron donor) to PMS (electron acceptor) through efficient electron transfer mediation by HOPC. The

DOI: 10.1021/acs.est.9b03067
Environ. Sci. Technol. 2019, 53, 10352−10360

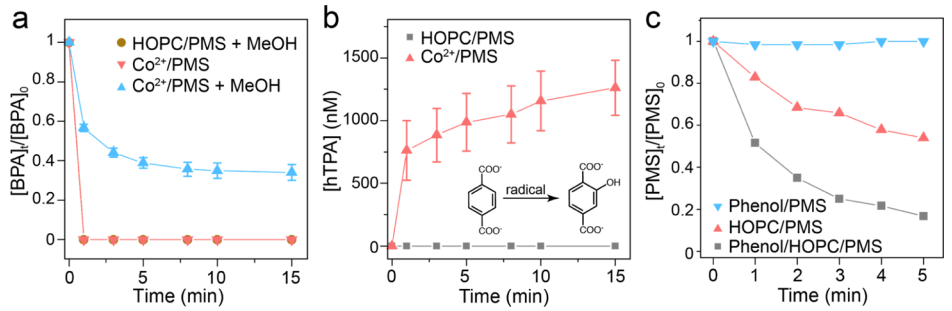

Figure 6. (a) Inhibition of BPA degradation by methanol ([BPA] = 50 μM), [HOPC] = 0.2 g/L. [Co^{2+}] = 2 mM, [PMS] = 2 mM, [methanol] = 2% v/v, and T = 20 °C. (b) Formation kinetics of hTPA ([TPA] = 1 mM, [HOPC] = 0.2 g/L or [Co^{2+}] = 2 mM, [PMS] = 2 mM, and T = 20 °C). (c) PMS degradation kinetics: [phenol] = 0.6 mM, if applicable, [HOPC] = 0.2 g/L, if applicable, [PMS] = 2 mM, and T = 20 °C.

HOPC-mediated electron transfer process was supported by significantly enhanced PMS decomposition upon addition of phenol as an electron donor (Text S4). In comparison, negligible PMS decomposition by direct reaction with phenol was observed in the absence of HOPC as an electron shuttle (Figure 6c), which is kinetically unfavorable under acidic pH.[40] The ordered porous structure and high surface area of HOPC ensure efficient mass transport and adsorption of the micropollutant and PMS, which is critical for the efficient electron transfer from micropollutants to PMS.[41,42] We further found that HOPC can efficiently adsorb PMS by 53% within 1 min (Text S5). Only minor adsorption of PMS was observed for CNT and rGO (Figure S5).

The unique electronic structure of HOPC, as modified by constitutional N, is likely to play a key role in rapid degradation of pollutants via electron transfer mediation. XPS analysis indicates that N atoms in HOPC are mainly comprised of aromatic N, including 27.5% of graphitic N, 21.9% of pyrrolic N, and 33.2% of pyridinic N. Previous studies suggest that these aromatic N atoms can induce electron transfer from adjacent C and impart a relatively high positive charge density on C atoms in CNT.[43−45] Instead of forming a regular end-on adsorption, peroxide may adsorb on positively charged C in a side-on mode (Scheme 1a).[44] The diatomic adsorption may significantly weaken the O−O bonding and facilitate the reductive activation of persulfate, which accordingly accelerates the electron transfer and oxidation of adsorbed micropollutants (Scheme 1b).

We note that HOPC could degrade PMS in the absence of an electron donor (Figure 6c), indicating the existence of a secondary nonradical PMS activation pathway other than electron transfer processes. Previous studies suggest singlet oxygen ($^1O_2$) as a potential product of automatic[30] or catalyzed[17,36] activation of PMS. Nevertheless, here the contribution of $^1O_2$ (if produced) to pollutant degradation is likely negligible because of the low reactivity of $^1O_2$ with the tested micropollutants (e.g., second-order rate constant = 3.0×10^5 M^{-1} s^{-1} for BPA,[46] that is, with 50 μM BPA, pseudo-first-order rate constant = 1.5×10^1 s^{-1}) and rapid quenching of $^1O_2$ by water (water-quenching rate constant = 2.5×10^5 s^{-1}). For instance, our calculation shows that in the HOPC/PMS/BPA system, 99.994% of $^1O_2$ would be physically quenched by water [assuming water and BPA as the only two quenchers; 2.5×10^5 s^{-1}/(1.5×10^1 s^{-1} + 2.5×10^5 s^{-1}) = 99.994%]. Assuming a maximum $^1O_2$ yield of 100% by PMS decay,[30] 0.34 mM PMS degradation observed at 1 min (Figure 6c) would generate 0.17 mM $^1O_2$, resulting in a maximum BPA degradation of 0.02 μM; this is much lower than the observed

Scheme 1. (a) Proposed Modified Peroxide Adsorption Model for the N-Doped Structure; (b) HOPC-Mediated Electron Transfer from Adsorbed Pollutants to PMS

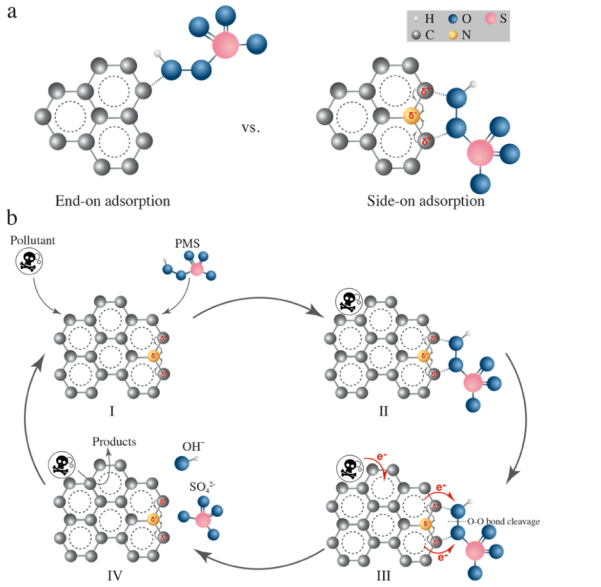

full degradation of 50 μM BPA (Figure 4a). The minor contribution of $^1O_2$ to contaminant degradation was further supported by unaffected BPA degradation upon addition of 2 mM histidine, a well-known selective $^1O_2$ quencher (addition of 20 mM histidine results in a calculated quenched $^1O_2$ concentration by 84%;[47,48] see Text S6). Finally, no degradation of furfuryl alcohol, a widely used $^1O_2$ probe,[47,48] was observed (Figure S6). All the above results strongly suggest a negligible contribution of $^1O_2$ to pollutant degradation in the HOPC/PMS system.

HOPC Exhibit Superior Pollutant Removal under Complex Water Matrix. This study demonstrates that HOPC can rapidly adsorb aqueous micropollutants and efficiently activate persulfate for pollutant degradation. The pollutant degradation mechanism does not involve generation of radicals; therefore, HOPC is not oxidized over repetitive use. In addition, the performance of a nonradical-based HOPC/PMS system is likely to be less hindered by the presence of water components (e.g., NOM) compared to radical-based systems. For instance, addition of radical-scavenging NOM did not inhibit BPA degradation, which contrasts to other radical-mediated oxidation processes (e.g., $^{\bullet}$OH-based processes in UV/TiO_2 and UV/H_2O_2 systems)

DOI: 10.1021/acs.est.9b03067
Environ. Sci. Technol. 2019, 53, 10352−10360

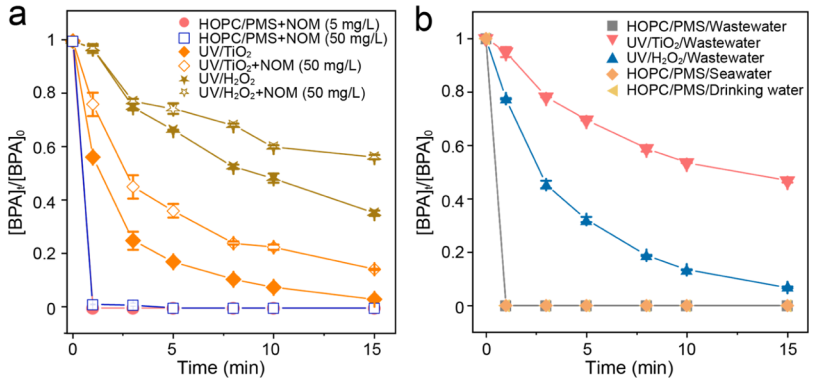

Figure 7. (a) Effect of NOM on BPA degradation in HOPC/PMS ([HOPC] = 0.2 g/L and [PMS] = 2 mM), UV/TiO_2 ([TiO_2] = 0.2 g/L), and UV/H_2O_2 ([H_2O_2] = 2 mM) reaction systems ([BPA] = 50 μM, [NOM] = 5 or 50 mg/L, UV irradiation (254 nm) = 2.6 mW/cm^2 (if applicable), and T = 20 °C). (b) BPA degradation kinetics under complex water conditions ([BPA] = 50 μM, [HOPC] = 0.2 g/L, [PMS] = 2 mM, and T = 20 °C). Composition of artificial drinking water is as follows: pH 7.6 (no change with PMS addition), 2 mg/L NOM, 252 mg/L $NaHCO_3$, 147 mg/L $CaCl_2{\cdot}2H_2O$, 124 mg/L $MgSO_4{\cdot}7H_2O$, 95 mg/L $Na_2SiO_3{\cdot}9H_2O$, 12 mg/L $NaNO_3$, 2.3 mg/L NaF, 0.18 mg/L $NaH_2PO_4{\cdot}H_2O$, and 5 mg/L NOM. Turbidity was adjusted to 5 NTU using bentonite clay. Artificial seawater composition: pH 8.2 (no change with PMS addition), 245 mg/L NaCl, 0.82 mg/L NaBr, 41 mg/L Na_2SO_4, 110 mg/L $MgCl_2{\cdot}6H_2O$, 16 mg/L $CaCl_2{\cdot}2H_2O$, 7.5 mg/L KCl, 0.22 mg/L H_3BO_3, 1.5 mg/L $NaHCO_3$, and 0.28 mg/L Na_2CO_3. Wastewater treatment plant effluent (pH 7.1 (decreased to 4.5 with PMS addition), BOD 17.9 mg/L, absorption spectrum shown in Figure S7) was collected from the East Shore Water Pollution Abatement Facility, New Haven, Connecticut on March 26, 2019.

where the pollutant removal rates were significantly affected by the presence of NOM (Figure 7a).[49,50] HOPC also exhibited excellent performance for BPA degradation in synthetic drinking water and seawater (Figure 7b). When an effluent water sample obtained from a wastewater plant was tested, BPA degradation also remained effective, with negligible impact on the kinetics (Figure 7b), outperforming radical-based systems, such as UV/TiO_2 and UV/H_2O_2 systems [Text S7 and S8; UV experiments were operated under typical conditions[8] using two 254 nm bulbs (8 W) and 0.2 g/L TiO_2 or 2 mM H_2O_2 (same peroxide concentration as PMS applied in this study)]. Here, the uniform pores of HOPC (~11 nm) may provide size exclusion of colloidal water components (e.g., NOM and soluble microbial products) such that inner pores, which provide a majority of surface area, continue to function as catalytic sites. The potential size exclusion and competitive adsorption toward pollutants require additional in-depth study on a wide range of target pollutants and water matrices. In addition, rapid degradation of BPA in water matrices spanning a wide pH range (i.e., pH ranging from 3.5 to 8.2 in above experiments) demonstrates the high pH versatility of the PMS/HOPC system.

Utilizing HOPC to enable nonradical oxidation pathway also allows overcoming known challenges of persulfate-based oxidation. In these applications, note that PMS applied at relatively low concentrations (i.e., 2 mM) would lead to generation of 192 mg/L sulfate as the decomposition product,[21] which is much lower than the EPA/CDC health advisory level in drinking water (500 mg/L).[51] In addition, the formation of toxic halogenated organic compounds and inorganic byproducts (e.g., chlorate), which is a significant concern in radical-based oxidation processes due to halogen radicals (e.g., Cl$^{\bullet}$) generation by reaction of $SO_4^{\bullet-}$ or $^{\bullet}$OH with halogen ions (e.g., Cl^-),[37] would be largely inhibited in the HOPC/PMS system due to lack of radical formation. Although a significant extent of mineralization was observed with BPA by HOPC/PMS, it remains to be determined whether persulfate-driven nonradical treatment can oxidize as a wide range of pollutants as conventional $^{\bullet}$OH-based AOPs and what types of oxidation byproducts form. Further studies including the pilot-scale test are needed to validate the feasibility of HOPC/PMS for the pursuit of highly espoused "hook and destroy" strategy, that is, cooperative coupling of adsorption and oxidation.

■ ASSOCIATED CONTENT

Supporting Information

The Supporting Information is available free of charge on the ACS Publications website at DOI: 10.1021/acs.est.9b03067.

Supporting figures, tables, detailed experimental methods, and the results of additional experiments (PDF)

■ AUTHOR INFORMATION

Corresponding Authors

*E-mail: aqwang@dicp.ac.cn (A.W.).
*E-mail: jaehong.kim@yale.edu (J.-H.K.).

ORCID

Chiheng Chu: 0000-0001-9493-9120
Jianfeng Li: 0000-0003-1598-6856
Aiqin Wang: 0000-0003-4552-0360
Pedro J. J. Alvarez: 0000-0002-6725-7199
Jae-Hong Kim: 0000-0003-2224-3516

Author Contributions

#C.C. and J.Y. contributed equally

Notes

The authors declare no competing financial interest.

■ ACKNOWLEDGMENTS

We acknowledge and appreciate partial support from the National Science Foundation Nanosystems Engineering Research Center for Nanotechnology-Enabled Water Treatment (EEC-1449500). We are grateful to C. Fausey (Yale) for BET measurements, to M. Sun (Yale) for CNT modification, and to X. Zhou (Yale) for XPS measurements.

■ REFERENCES

(1) Stuetz, R.; International Water Association. *Principles of Water and Wastewater Treatment Processes*; IWA Publishing: London, 2009.

DOI: 10.1021/acs.est.9b03067
Environ. Sci. Technol. 2019, 53, 10352−10360

(2) Ali, I.; Gupta, V. K. Advances in Water Treatment by Adsorption Technology. *Nat. Protoc.* **2007**, *1*, 2661.
(3) Sabio, E.; González, E.; González, J. F.; González-García, C. M.; Ramiro, A.; Gañan, J. Thermal Regeneration of Activated Carbon Saturated with p-Nitrophenol. *Carbon* **2004**, *42*, 2285−2293.
(4) Alsbaiee, A.; Smith, B. J.; Xiao, L.; Ling, Y.; Helbling, D. E.; Dichtel, W. R. Rapid removal of organic micropollutants from water by a porous β-cyclodextrin polymer. *Nature* **2016**, *529*, 190−194.
(5) Navalon, S.; Dhakshinamoorthy, A.; Alvaro, M.; Garcia, H. Heterogeneous Fenton Catalysts Based on Activated Carbon and Related Materials. *ChemSusChem* **2011**, *4*, 1712−1730.
(6) Hu, P.; Long, M. Cobalt-Catalyzed Sulfate Radical-Based Advanced Oxidation: A Review on Heterogeneous Catalysts and Applications. *Appl. Catal., B* **2016**, *181*, 103−117.
(7) Brame, J.; Long, M.; Li, Q.; Alvarez, P. Trading Oxidation Power for Efficiency: Differential Inhibition of Photo-Generated Hydroxyl Radicals versus Singlet Oxygen. *Water Res.* **2014**, *60*, 259−266.
(8) Lee, C.-G.; Javed, H.; Zhang, D.; Kim, J.-H.; Westerhoff, P.; Li, Q.; Alvarez, P. J. J. Porous Electrospun Fibers Embedding TiO_2 for Adsorption and Photocatalytic Degradation of Water Pollutants. *Environ. Sci. Technol.* **2018**, *52*, 4285−4293.
(9) Zhang, D.; Lee, C.; Javed, H.; Yu, P.; Kim, J.-H.; Alvarez, P. J. J. Easily Recoverable, Micrometer-Sized TiO_2 Hierarchical Spheres Decorated with Cyclodextrin for Enhanced Photocatalytic Degradation of Organic Micropollutants. *Environ. Sci. Technol.* **2018**, *52*, 12402−12411.
(10) Alvarez, P. J. J.; Chan, C. K.; Elimelech, M.; Halas, N. J.; Villagrán, D. Emerging Opportunities for Nanotechnology to Enhance Water Security. *Nat. Nanotechnol.* **2018**, *13*, 634−641.
(11) Hartmann, M.; Kullmann, S.; Keller, H. Wastewater Treatment with Heterogeneous Fenton-Type Catalysts Based on Porous Materials. *J. Mater. Chem.* **2010**, *20*, 9002−9017.
(12) Halim, A. A.; Aziz, H. A.; Johari, M. A. M.; Ariffin, K. S. Comparison Study of Ammonia and Cod Adsorption on Zeolite, Activated Carbon and Composite Materials in Landfill Leachate Treatment. *Desalination* **2010**, *262*, 31−35.
(13) Wacławek, S.; Lutze, H. V.; Grübel, K.; Padil, V. V. T.; Černík, M.; Dionysiou, D. D. Chemistry of Persulfates in Water and Wastewater Treatment: A Review. *Chem. Eng. J.* **2017**, *330*, 44−62.
(14) Duan, X.; Sun, H.; Kang, J.; Wang, Y.; Indrawirawan, S.; Wang, S. Insights into Heterogeneous Catalysis of Persulfate Activation on Dimensional-Structured Nanocarbons. *ACS Catal.* **2015**, *5*, 4629−4636.
(15) Lee, H.; Kim, H.-i.; Weon, S.; Choi, W.; Hwang, Y. S.; Seo, J.; Lee, C.; Kim, J.-H. Activation of Persulfates by Graphitized Nanodiamonds for Removal of Organic Compounds. *Environ. Sci. Technol.* **2016**, *50*, 10134−10142.
(16) Guan, C.; Jiang, J.; Pang, S.; Luo, C.; Ma, J.; Zhou, Y.; Yang, Y. Oxidation Kinetics of Bromophenols by Nonradical Activation of Peroxydisulfate in the Presence of Carbon Nanotube and Formation of Brominated Polymeric Products. *Environ. Sci. Technol.* **2017**, *51*, 10718−10728.
(17) Yun, E.-T.; Lee, J. H.; Kim, J.; Park, H.-D.; Lee, J. Identifying the Nonradical Mechanism in the Peroxymonosulfate Activation Process: Singlet Oxygenation Versus Mediated Electron Transfer. *Environ. Sci. Technol.* **2018**, *52*, 7032−7042.
(18) Yun, E.-T.; Yoo, H.-Y.; Bae, H.; Kim, H.-I.; Lee, J. Exploring the Role of Persulfate in the Activation Process: Radical Precursor versus Electron Acceptor. *Environ. Sci. Technol.* **2017**, *51*, 10090−10099.
(19) Duan, X.; Ao, Z.; Zhou, L.; Sun, H.; Wang, G.; Wang, S. Occurrence of Radical and Nonradical Pathways from Carbocatalysts for Aqueous and Nonaqueous Catalytic Oxidation. *Appl. Catal., B* **2016**, *188*, 98−105.
(20) Duan, X.; Sun, H.; Wang, S. Metal-Free Carbocatalysis in Advanced Oxidation Reactions. *Acc. Chem. Res.* **2018**, *51*, 678−687.
(21) Hu, P.; Su, H.; Chen, Z.; Yu, C.; Li, Q.; Zhou, B.; Alvarez, P. J. J.; Long, M. Selective Degradation of Organic Pollutants Using an Efficient Metal-Free Catalyst Derived from Carbonized Polypyrrole Via Peroxymonosulfate Activation. *Environ. Sci. Technol.* **2017**, *51*, 11288−11296.
(22) Yang, K.; Wang, J.; Chen, X.; Zhao, Q.; Ghaffar, A.; Chen, B. Application of Graphene-Based Materials in Water Purification: From the Nanoscale to Specific Devices. *Environ. Sci.: Nano* **2018**, *5*, 1264−1297.
(23) Zhang, S.; Shao, T.; Bekaroglu, S. S. K.; Karanfil, T. The Impacts of Aggregation and Surface Chemistry of Carbon Nanotubes on the Adsorption of Synthetic Organic Compounds. *Environ. Sci. Technol.* **2009**, *43*, 5719−5725.
(24) Shen, Y.; Fang, Q.; Chen, B. Environmental Applications of Three-Dimensional Graphene-Based Macrostructures: Adsorption, Transformation, and Detection. *Environ. Sci. Technol.* **2015**, *49*, 67−84.
(25) Zhao, Y.; Watanabe, K.; Hashimoto, K. Self-Supporting Oxygen Reduction Electrocatalysts Made from a Nitrogen-Rich Network Polymer. *J. Am. Chem. Soc.* **2012**, *134*, 19528−19531.
(26) Chen, H.; Carroll, K. C. Metal-Free Catalysis of Persulfate Activation and Organic-Pollutant Degradation by Nitrogen-Doped Graphene and Aminated Graphene. *Environ. Pollut.* **2016**, *215*, 96−102.
(27) Vázquez-Santos, M. B.; Geissler, E.; László, K.; Rouzaud, J.-N.; Martínez-Alonso, A.; Tascón, J. M. D. Comparative XRD, Raman, and TEM Study on Graphitization of PbO-Derived Carbon Fibers. *J. Phys. Chem. C* **2012**, *116*, 257−268.
(28) Liu, W.; Zhang, L.; Yan, W.; Liu, X.; Yang, X.; Miao, S.; Wang, W.; Wang, A.; Zhang, T. Single-Atom Dispersed Co-N-C Catalyst: Structure Identification and Performance for Hydrogenative Coupling of Nitroarenes. *Chem. Sci.* **2016**, *7*, 5758−5764.
(29) Liu, W.; Zhang, L.; Liu, X.; Liu, X.; Yang, X.; Miao, S.; Wang, W.; Wang, A.; Zhang, T. Discriminating Catalytically Active FeNx Species of Atomically Dispersed Fe-N-C Catalyst for Selective Oxidation of the C-H Bond. *J. Am. Chem. Soc.* **2017**, *139*, 10790−10798.
(30) Yang, Y.; Banerjee, G.; Brudvig, G. W.; Kim, J.-H.; Pignatello, J. J. Oxidation of Organic Compounds in Water by Unactivated Peroxymonosulfate. *Environ. Sci. Technol.* **2018**, *52*, 5911−5919.
(31) Anipsitakis, G. P.; Dionysiou, D. D. Radical Generation by the Interaction of Transition Metals with Common Oxidants. *Environ. Sci. Technol.* **2004**, *38*, 3705−3712.
(32) Anipsitakis, G. P.; Dionysiou, D. D. Degradation of Organic Contaminants in Water with Sulfate Radicals Generated by the Conjunction of Peroxymonosulfate with Cobalt. *Environ. Sci. Technol.* **2003**, *37*, 4790−4797.
(33) Dogliotti, L.; Hayon, E. Flash photolysis of per[oxydi]sulfate ions in aqueous solutions. The sulfate and ozonide radical anions. *J. Phys. Chem.* **1967**, *71*, 2511−2516.
(34) Buxton, G. V.; Greenstock, C. L.; Helman, W. P.; Ross, A. B. Critical-Review of Rate Constants for Reactions of Hydrated Electrons, Hydrogen-Atoms and Hydroxyl Radicals ($^{\cdot}OH/^{\cdot}O^{-}$) in Aqueous-Solution. *J. Phys. Chem. Ref. Data* **1988**, *17*, 513−886.
(35) Neta, P.; Madhavan, V.; Zemel, H.; Fessenden, R. W. Rate Constants and Mechanism of Reaction of Sulfate Radical Anion with Aromatic Compounds. *J. Am. Chem. Soc.* **1977**, *99*, 163−164.
(36) Zhu, S.; Li, X.; Kang, J.; Duan, X.; Wang, S. Persulfate Activation on Crystallographic Manganese Oxides: Mechanism of Singlet Oxygen Evolution for Nonradical Selective Degradation of Aqueous Contaminants. *Environ. Sci. Technol.* **2018**, *53*, 307−315.
(37) Zhang, W.; Zhou, S.; Sun, J.; Meng, X.; Luo, J.; Zhou, D.; Crittenden, J. Impact of Chloride Ions on UV/H_2O_2 and UV/Persulfate Advanced Oxidation Processes. *Environ. Sci. Technol.* **2018**, *52*, 7380−7389.
(38) Ahn, Y.-Y.; Yun, E.-T.; Seo, J.-W.; Lee, C.; Kim, S. H.; Kim, J.-H.; Lee, J. Activation of Peroxymonosulfate by Surface-Loaded Noble Metal Nanoparticles for Oxidative Degradation of Organic Compounds. *Environ. Sci. Technol.* **2016**, *50*, 10187−10197.
(39) Page, S. E.; Arnold, W. A.; McNeill, K. Terephthalate as a Probe for Photochemically Generated Hydroxyl Radical. *J. Environ. Monit.* **2010**, *12*, 1658−1665.

DOI: 10.1021/acs.est.9b03067
Environ. Sci. Technol. 2019, 53, 10352−10360

(40) Goodman, J. F.; Robson, P. 534. Decomposition of inorganic peroxyacids in aqueous alkali. *J. Chem. Soc.* **1963**, 2871−2875.
(41) Zhu, S.; Huang, X.; Ma, F.; Wang, L.; Duan, X.; Wang, S. Catalytic Removal of Aqueous Contaminants on N-Doped Graphitic Biochars: Inherent Roles of Adsorption and Nonradical Mechanisms. *Environ. Sci. Technol.* **2018**, *52*, 8649−8658.
(42) Zhang, T.; Chen, Y.; Wang, Y.; Le Roux, J.; Yang, Y.; Croué, J.-P. Efficient Peroxydisulfate Activation Process Not Relying on Sulfate Radical Generation for Water Pollutant Degradation. *Environ. Sci. Technol.* **2014**, *48*, 5868−5875.
(43) Zhao, Y.; Yang, L.; Chen, S.; Wang, X.; Ma, Y.; Wu, Q.; Jiang, Y.; Qian, W.; Hu, Z. Can Boron and Nitrogen Co-Doping Improve Oxygen Reduction Reaction Activity of Carbon Nanotubes? *J. Am. Chem. Soc.* **2013**, *135*, 1201−1204.
(44) Gong, K.; Du, F.; Xia, Z.; Durstock, M.; Dai, L. Nitrogen-Doped Carbon Nanotube Arrays with High Electrocatalytic Activity for Oxygen Reduction. *Science* **2009**, *323*, 760−764.
(45) Tang, Y.; Allen, B. L.; Kauffman, D. R.; Star, A. Electrocatalytic Activity of Nitrogen-Doped Carbon Nanotube Cups. *J. Am. Chem. Soc.* **2009**, *131*, 13200−13201.
(46) Arnold, W. A.; Oueis, Y.; O'Connor, M.; Rinaman, J. E.; Taggart, M. G.; McCarthy, R. E.; Foster, K. A.; Latch, D. E. QSARs for phenols and phenolates: oxidation potential as a predictor of reaction rate constants with photochemically produced oxidants. *Environ. Sci.: Processes Impacts* **2017**, *19*, 324−338.
(47) Chu, C.; Erickson, P. R.; Lundeen, R. A.; Stamatelatos, D.; Alaimo, P. J.; Latch, D. E.; McNeill, K. Photochemical and Nonphotochemical Transformations of Cysteine with Dissolved Organic Matter. *Environ. Sci. Technol.* **2016**, *50*, 6363−6373.
(48) Chu, C.; Lundeen, R. A.; Remucal, C. K.; Sander, M.; McNeill, K. Enhanced Indirect Photochemical Transformation of Histidine and Histamine through Association with Chromophoric Dissolved Organic Matter. *Environ. Sci. Technol.* **2015**, *49*, 5511−5519.
(49) Lindsey, M. E.; Tarr, M. A. Inhibition of Hydroxyl Radical Reaction with Aromatics by Dissolved Natural Organic Matter. *Environ. Sci. Technol.* **2000**, *34*, 444−449.
(50) Westerhoff, P.; Aiken, G.; Amy, G.; Debroux, J. Relationships between the Structure of Natural Organic Matter and Its Reactivity Towards Molecular Ozone and Hydroxyl Radicals. *Water Res.* **1999**, *33*, 2265−2276.
(51) EPA. *Contaminant Candidate List Regulatory Determination Support Document for Sulfate*, 2003.

DOI: 10.1021/acs.est.9b03067
Environ. Sci. Technol. 2019, 53, 10352−10360